fluorobenzoate, 80079-06-7; 3-*tert*-butylphenyl *p*-fluorobenzoate, 90172-31-9; *m*-methoxyphenyl *p*-fluorobenzoate, 90172-32-0; *p*-methoxyphenyl *p*-fluorobenzoate, 80079-00-1; resorcinyl di-*p*-fluorobenzoate, 90172-33-1; 1,2-phenylene di-*p*-fluorobenzoate, 90172-34-2; *m*-chlorophenyl *p*-fluorobenzoate, 90172-35-3; *o*-chlorophenyl *p*-fluorobenzoate, 90172-36-4; *o*-nitrophenyl *p*-fluorobenzoate, 90172-37-5; *m*-nitrophenyl *p*-fluorobenzoate, 2710-17-0; *p*-nitrophenyl *p*-fluorobenzoate, 2710-18-1; *o*-bromophenyl *p*-fluorobenzoate, 90172-38-6; *m*-bromophenyl *p*-fluorobenzoate, 90172-39-7; *p*-bromophenyl *p*-fluorobenzoate, 656-21-3; 1-naphthyl *p*-fluorobenzoate, 90172-40-0; 2-naphthyl *p*-fluorobenzoate, 90172-41-1; benzoic acid anhydride with *p*-fluorobenzoic acid, 1800-04-0; *p*-nitrobenzoic acid anhydride with *p*-fluorobenzoic acid, 90172-42-2; *m*-bromobenzoic acid anhydride with *p*-fluorobenzoic acid, 90172-43-3; *p*-bromobenzoic acid anhydride with *p*-fluorobenzoic acid, 90172-44-4; *o*-chlorobenzoic acid anhydride with *p*-fluorobenzoic acid, 90172-45-5; *m*-chlorobenzoic acid anhydride with *p*-fluorobenzoic acid, 90172-46-6; *p*-chlorobenzoic acid anhydride with *p*-fluorobenzoic acid, 25569-91-9; diphenylacetic acid anhydride with *p*-fluorobenzoic acid, 90172-47-7; triphenylacetic acid anhydride with *p*-fluorobenzoic acid, 90172-48-8; (2-naphthoxy)acetic acid anhydride with *p*-fluorobenzoic acid, 90172-49-9; anthracene-9-carboxylic acid anhydride with *p*-fluorobenzoic acid, 90172-50-2; 1-naphthoic acid anhydride with *p*-fluorobenzoic acid, 90172-51-3; 2-naphthoic acid anhydride with *p*-fluorobenzoic acid, 90172-52-4; 3-hydroxy-2-naphthoic acid anhydride with *p*-fluorobenzoic acid, 90172-53-5; *N*-*n*-butyl-*p*-fluorobenzamide, 3851-81-8; *p*-fluoro-*N*-isobutylbenzamide, 88358-25-2; *p*-fluoro-*N*-*sec*-butylbenzamide, 90172-54-6; *p*-fluoro-*N*-*tert*-butylbenzamide, 49834-29-9; *p*-fluoro-*N*-phenethylbenzamide, 33799-96-1; *p*-fluoro-*N*-phenylbenzamide, 366-63-2; *N*-benzyl-*p*-fluorobenzamide, 725-38-2; *N*,*N*-diphenyl-*p*-fluorobenzamide, 79606-49-8; 1-(*p*-fluorophenylcarbonyl)-2,2,6,6-tetramethylpiperidine, 90172-55-7; *N*-*n*-butyl-*N*-ethyl-*p*-fluorobenzamide, 90172-56-8; *N*,*N*-di-*n*-butyl-*p*-fluorobenzamide, 90172-57-9; *N*,*N*-diethyl-*p*-fluorobenzamide, 10366-88-8; 1,4-bis(*p*-fluorophenylcarbonyl)hexahydro-1,4-diazepine, 90172-58-0; 9-(*p*-fluorophenylcarbonyl)-10,11-dihydro-5*H*-dibenz[*b*,*f*]azepine, 90172-59-1; *N*,*N*-diisopropyl-*p*-fluorobenzamide, 24167-56-4; *p*-fluoro-*N*-methylbenzamide, 701-49-5; 1-(*p*-fluorophenylcarbonyl)indoline, 90172-60-4; *p*-fluoro-*N*-phenyl-*N*-(phenylcarbonyl)benzamide, 90193-57-0; 1-(*p*-fluorophenylcarbonyl)-pyrrole, 90172-61-5; 9-(*p*-fluorophenylcarbonyl)carbazole, 90172-62-6; 1-(*p*-fluorophenylcarbonyl)imidazole, 90172-63-7; 1-(*p*-fluorophenylcarbonyl)-2-methylimidazole, 90172-64-8; 2-ethyl-1-(*p*-fluorophenylcarbonyl)-4-methylimidazole, 90172-65-9; 1-(*p*-fluorophenylcarbonyl)indole, 90172-66-0; 1-(*p*-fluorophenylcarbonyl)indole-2,3-dione, 90172-67-1; 1-(*p*-fluorophenylcarbonyl)indazole, 90172-68-2; *N*,*N*′-bis(*p*-fluorophenylcarbonyl)urea, 90172-69-3; 1-hexanethiol *p*-fluorobenzoate, 90172-70-6; 2-propanethiol *p*-fluorobenzoate, 90172-71-7; benzyl mercaptan *p*-fluorobenzoate, 90172-72-8; thiophenol *p*-fluorobenzoate, 90172-73-9; *p*-thiocresol *p*-fluorobenzoate, 90172-74-0; thiolacetic acid anhydride with *p*-fluorobenzoic acid, 90172-75-1.

LITERATURE CITED

(1) Sleevi, P.; Glass, T. E.; Dorn, H. C. *Anal. Chem.* **1979**, *51*, 1931–1934.
(2) Manatt, S. L. *J. Am. Chem. Soc.* **1966**, *88*, 1323–1324.
(3) Konishi, K.; Mori, Y.; Taniguchi, N. *Analyst (London)* **1969**, *94*, 1002–1005.
(4) Manatt, S. L.; Lawson, D. D.; Ingham, J. D.; Rapp, N. S.; Hardy, J. P. *Anal. Chem.* **1966**, *38*, 1063–1065.
(5) Voelter, W.; Brietmaler, E.; Jung, G.; Bayer, E. *Org. Magn. Reson.* **1970**, *2*, 251–257.
(6) Konishi, K.; Kanoh, Y. *Anal. Chem.* **1968**, *40*, 1881–1883.
(7) Jung, G.; Voelter, W.; Brietmaler, W.; Bayer, E. *Tetrahedron Lett.* **1969**, *39*, 3785–3788.
(8) Leader, G. R. *Anal. Chem.* **1970**, *42*, 16–21.
(9) Leader, G. R. *Anal. Chem.* **1973**, *45*, 1700–1706.
(10) Ho, F. F.-L. *Anal. Chem.* **1973**, *45*, 603–605.
(11) Ho, F. F.-L. *Anal. Chem.* **1974**, *46*, 496.
(12) Ho, F. F.-L.; Rohler, R. R. *Anal. Chem.* **1974**, *46*, 1302–1304.
(13) Leader, G. R. *Appl. Spectrosc. Rev.* **1976**, *11*, 287–317.
(14) Koller, K. L.; Dorn, H. C. *Anal. Chem.* **1982**, *54*, 529–533.
(15) Zuber, G. E.; Staiger, D. B.; Warren, R. J. *Anal. Chem.* **1983**, *55*, 64–67.
(16) Shue, F. F.; Yen, T. F. *Anal. Chem.* **1982**, *54*, 1641–1642.
(17) Manatt, S. L., et al. *Tetrahedron Lett.* **1980**, *21*, 1397–1400.
(18) Taft, R. W.; Prosser, F.; Goodman, L.; Davis, G. T. *J. Chem. Phys.* **1963**, *38*, 380–387.

RECEIVED for review January 3, 1984. Accepted March 22, 1984.

Depth Resolved Spectroscopic Analysis of Solid Samples Using Photoacoustic Spectroscopy

Gordon F. Kirkbright,[1] Richard M. Miller,* and Dominic E. M. Spillane

Department of Instrumentation and Analytical Science, University of Manchester Institute of Science and Technology, P.O. Box 88, Manchester M60 1QD, United Kingdom

Yoshinori Sugitani

Institute of Chemistry, University of Tsukuba, Sakura-mura, Ibaraki 305, Japan

The use of impulse response measurements for signal recovery in photoacoustic spectroscopy is described. The technique is compared with the use of sequential single frequency modulation methods and is shown to give improved results in depth profiling studies. An instrument capable of performing impulse response photoacoustic spectroscopy (IMPAS) is described and applied to a number of multilayer samples.

[1] Deceased.

There are many areas in which the ability to study the distribution of chromophores within solid or quasi-solid samples would be of considerable use; for example, the study of dyeing processes, the fabrication of multilayer materials, and the study of transport mechanisms in biological materials. A major claim for photoacoustic spectroscopy (PAS) has always been that it provides a nondestructive method of acquiring depth related spectroscopic information from solid samples. Despite this, very little has been reported in the literature on depth-profiling using PAS. It has been shown (*1–3*) that it is possible to discriminate between the waxy,

0003-2700/84/0356-2043$01.50/0 © 1984 American Chemical Society

cuticular layer of fruit rinds and leaves, and the pigment containing subcuticular layer. Studies have also been made of the distribution of materials within lobster shells (*4*) and of the structure of lichens (*5*). However, the difficulties of performing such experiments have limited their range of application. In conventional depth-profiling experiments, the photoacoustic spectrum is recorded at a number of modulation frequencies (*2*). The signal recorded at each frequency corresponds to the integrated photoacoustic signal from a different thickness of the sample, modified by loss mechanisms within the sample. At high modulation frequencies, the signal is derived from a thin section of the sample at the surface. As the frequency is reduced, the thickness of the sample contributing to the overall signal increases. Therefore, by recording the photoacoustic spectrum at a range of different modulation frequencies, an indication of the distribution of the absorbing species can be obtained. The combination of the difficulty of interpreting the data from such experiments and the rapid decrease in the signal to noise ratio of the photoacoustic signal with increasing frequency has meant that very little work on the practical applications of depth profiling has been performed.

Recent developments in this laboratory (*6*) and elsewhere (*7, 8*) have shown that impulse response measurements performed using multifrequency test signals, together with cross correlation signal recovery, produce depth-related signals which are both simpler to obtain and easier to interpret than conventional PAS data. A time-resolved impulse response can be used to develop a three-dimensional surface which describes the excitation wavelength, the amplitude of the photoacoustic signal, and the depth within the sample from which the signal originates.

In this paper we describe the construction of an instrument capable of performing impulse response photoacoustic spectroscopy (IMPAS). The instrument is used to study a number of sample systems containing depth information, and the results obtained are compared with those obtained by conventional PAS.

CROSS-CORRELATION TECHNIQUES

The use of cross correlation coupled with multifrequency test signals to measure the impulse response of a system under test has a long history in engineering (*9*). More recently it has also found applications in the measurement of time-resolved spectroscopic signals (*6–8, 10*). Compared to conventional signal impulse perturbation techniques, the use of multifrequency test signals provides a greatly improved signal to noise ratio for a given measurement time due to the increased duty cycle of the source. Correlation functions express the degree of similarity between two signals as they are gradually delayed by a time τ with respect to each other. A signal $x(t)$ compared with itself provides an autocorrelation function R_{xx} and the comparison of two signals $x(t)$ and $y(t)$ provides the cross-correlation function R_{xy}.

$$R_{xx}(\tau) = \frac{1}{T}\int_0^T x(t-\tau)\cdot x(t)\,dt \qquad (1)$$

$$R_{xy}(\tau) = \frac{1}{T}\int_0^T x(t-\tau)\cdot y(t)\,dt \qquad (2)$$

where T is the integration time and τ the delay time. It can be shown that the relationship between the impulse response of a system $h(t)$ and the cross-correlation function between the test signal applied to the system and the system response R_{iz} is given by the convolution integral

$$R_{iz}(\tau) = \int_0^{T_s} h(t)\cdot R_{ii}(\tau - t)\,dt + R_{in}(\tau) \qquad (3)$$

where T_s is the system settling time, R_{ii} is the autocorrelation function of the test signal and R_{in} is the cross-correlation function between the test signal and the system noise (*9*). If the noise is not well correlated with the test signal, averaging R_{in} over time will reduce it to a low level. If a test signal is used which has the same autocorrelation function as a simple impulse, then R_{iz} is directly proportional to the system impulse response $h(t)$.

A suitable test signal is the pseudo-random binary sequence (PRBS). The PRBS has two levels and can switch from one to the other only at certain time intervals. The probability of the sequence changing state at each time interval is 0.5. The sequence is fixed and reproducible, lasting N time intervals where N is an odd integer. Further details of the use of PRBS test signals and cross correlation for signal recovery in photoacoustic experiments are given elsewhere (*6*).

PRBS modulation can be imposed on a white light source by using a rotating metal disk with the PRBS sequence cut into it. A metal disk is divided into N segments, each corresponding to one element of the PRBS. The PRBS is then mapped onto the disk and sectors corresponding to one level of the PRBS removed and sectors corresponding to the other level of the PRBS left intact. When the disk is rotated in front of the light source the PRBS is imposed on the light source as a sequence of light and dark periods.

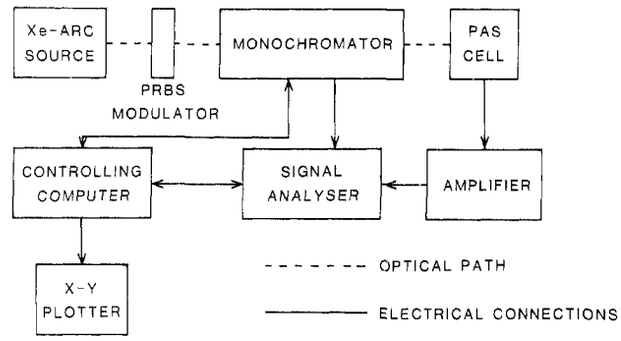

Figure 1. Block diagram of an impulse response photoacoustic spectrometer.

EXPERIMENTAL METHOD

Instrumentation. The spectrometer used for the photoacoustic studies reported in this paper has been described in detail elsewhere (*11*). Radiation from a 300-W xenon arc with an integral aluminum reflector (Type VIX 300, Varian Associates, Palo Alto, CA) was focused through a variable speed chopper (Model 9479, Brookdeal Electronics, Ltd., UK) by a silica lens onto the entrance slit of an $f/4$ grating monochromator (Metrospec, DGO, Ltd., UK). The transmitted radiation was folded down into a commercially available photoacoustic cell (Model OAS 401, EDT Research, Ltd., UK) using a front surface concave mirror. The spectral half-bandwidth of the transmitted radiation was 20 nm. The sample chamber of the cell has a usable area of 15 mm × 5 mm and is approximately 1 mm deep. The geometry of the sample chamber allows easy matching of the exit optics of the monochromator to the sample. Samples were cut to shape and laid loosely in the sample tray.

The signal from the cell, together with a reference signal generated by the modulation system, was taken to a lock-in amplifier (Model 9505E, E.G. & G. Brookdeal, Ltd., UK). The resulting photoacoustic signal was stored using a digital scan recorder (Model 4104, Princeton Applied Research Corp., Princeton, NJ). The wavelength of the incident beam was scanned with a stepper-motor drive controlled by a local oscillator. Photoacoustic spectra were recorded at a scan rate of 50 nm min^{-1} and with a lock-in amplifier time constant of 3 s. The resulting spectra were displayed on an oscilloscope and hard copy was obtained from an X-Y recorder. For the averaged measurements at a single wavelength, a digital signal averager was used (Model 4202, Princeton Applied Research Corp.).

In order to perform IMPAS measurements, the system was modified as shown in Figure 1. The optical train of the spec-

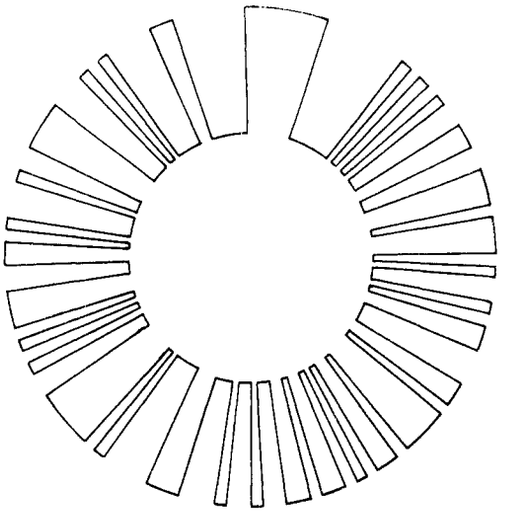

Figure 2. PRBS modulator disk.

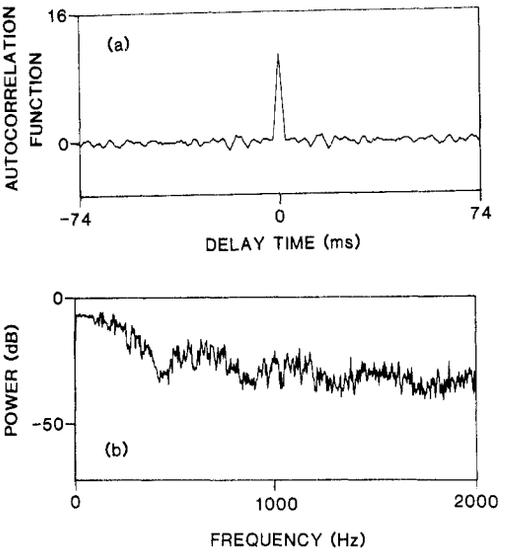

Figure 3. Power spectrum and autocorrelation function obtained from the PRBS modulator rotating at 3 Hz.

trometer was left essentially unchanged. The symmetrical rotating sector of the modulation system was replaced with a specially constructed PRBS sector described below. The sector was mounted so that the disk radius lay parallel to and through the center of the entrance slit of the monochromator, giving the minimum rise and fall times on the light pulses generated by the rotating sector. The reference signal was obtained by placing an optical fiber in the light path to lead a small portion of the modulated beam to a photodiode. The photoacoustic signal from the cell was preamplified (Model 750S, Brookdeal Electronics Ltd., UK) and taken, together with the reference signal, to a digital signal analyzer (Solartron 1200, Solartron Instruments, Ltd., UK) which performed the cross correlation. The signal analyzer has a maximum measurement bandwidth of 2 kHz in all the experiments described here to allow the measurement of impulse responses over an adequate time span. The signal analyzer and the monochromator drive were controlled by a laboratory instrumentation minicomputer (MINC 11/23, DEC, Ltd., UK). Experimental data were stored on disk for later analysis.

PRBS Modulator. The asymmetric rotating sector for IMPAS measurements was cut according to the design of Sugitani et al. (*8*). The design is based on an M-series pseudorandom sequence of zeroes and ones, 127 bits in length. The sequence was as follows:

0000001111111010101001100111011
1101001011000110111101101011011
1001001000111000010111111001010
1110011010001001111000101000011
1000001

A metal disk was marked off into 127 sectors and each sector corresponding to a "1" in the sequence removed. The central section of the disk was left uncut to allow the disk to be mounted on the drive shaft. Figure 2 shows a diagram of the cut disk.

Examination of the photodiode output while the sector was rotating at a steady speed showed that the PRBS sequence was being imposed on the white light source. Figure 3 shows the autocorrelation function and power spectrum of the modulation with the sector rotating at 3 Hz obtained by processing the output of the photodiode with the digital signal analyzer. For the cross-correlation function to be a good approximation of the system impulse response, the input autocorrelation function should be the same as that obtained for a simple impulse. The autocorrelation function of a simple impulse is a symmetric triangular function centered on zero time delay and with a half width at the base equal to the width of the impulse (*6*). Figure 3a shows that the PRBS modulation does have the desired properties, although there are some symmetric errors in the autocorrelation function at longer time delays which are probably due to imperfections in the cutting of the disk. Figure 3b shows the power spectrum of the modulation on a logarithmic scale. The power spectrum is close to the theoretical spectrum expected for such a sequence although somewhat noisy. This excess noise can be partially attributed to source noise in the xenon arc and to flaws in the PRBS sequence. The results obtained indicate that good quality impulse responses could be obtained with some signal averaging.

Signal Processing. As the spectrometer used was a single beam instrument, it was necessary to normalize the PAS data to correct for variations in the source power spectrum. For the conventional PAS measurements, the power spectrum was obtained by recording the photoacoustic spectrum of carbon black. Normalization was performed by dividing the experimental spectrum by the reference source power spectrum (*1*). For the IMPAS measurements a similar approach was used. A reference source power spectrum was recorded in conventional PAS mode and stored in the controlling computer as a table of wavelengths and corresponding signal amplitudes. As each cross correlation function was read into the computer from the digital signal analyzer, each point in the impulse response was divided by the appropriate signal amplitude for the wavelength being measured. The normalized impulse responses were then stored on disk for further processing and display.

After the IMPAS data had been normalized, they could be displayed locally on a digital X-Y plotter using simple graphics software or transferred to the local mainframe computer (CYBER 170/730, Control Data Corp., USA) for further analysis and display using the GINO-F graphics package.

All PAS and IMPAS signal amplitudes are quoted in terms of a consistent set of arbitrary units. Signal amplitudes in the various experiments are therefore directly comparable. The PAS data have not been scaled in a consistent fashion and the amplitudes can be compared only where this has been explicitly stated.

RESULTS AND DISCUSSION

In order to compare the relative merits of IMPAS and sequential single frequency PAS measurements as methods of obtaining depth-related information, two samples were prepared: (1) a matrix of poly(vinyl chloride) heavily doped with bromothymol blue, (The sample was planar and approximately 1 mm in thickness.); (2) a matrix of poly(urethane acrylate) doped with a lower concentration of the same dye (The sample was again planar and approximately 1 mm thick. The surface of this sample was coated with a thin layer of blue pigment.).

Figure 4a shows the photoacoustic spectrum of sample 1 in the range 300–720 nm for four different modulation frequencies between 15 Hz and 90 Hz. There are two main absorption features in this region of the spectrum centered at approximately 412 nm and 560 nm. The higher energy feature may be assigned to absorption by bromothymol blue. The lower energy feature was found to appear only when a high concentration of the dye was used and is assumed to arise from association of the dye molecules.

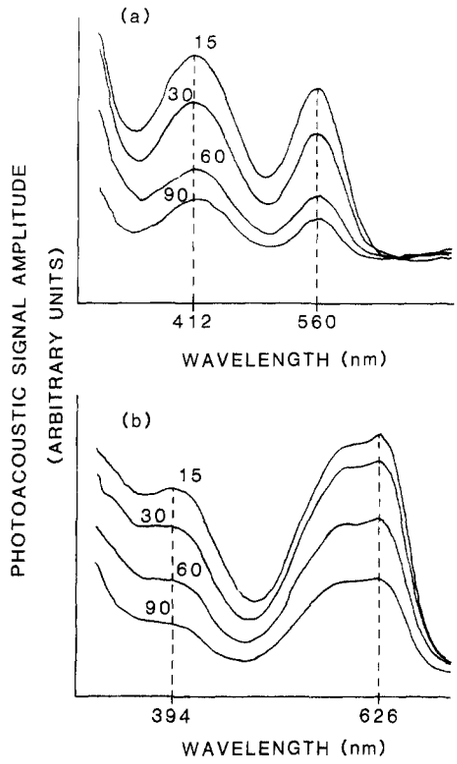

Figure 4. Photoacoustic spectrum of dyed polymer films at modulation frequencies of 15, 30, 60, and 90 Hz: (a) bulk-dyed polymer film, (b) bulk-dyed polymer film with a surface coating.

Figure 4b shows the photoacoustic spectrum of sample 2 over the same range of wavelengths and modulation frequencies. Investigations prior to the application of the blue coating indicated that the dye–polymer sample shows no significant absorption above 500 nm. The large absorption feature centered at 584 nm and 626 nm may therefore be assumed to arise solely from the coating. The band centered at 394 nm is assumed to arise from the bromothymol blue; the slight shift in absorption maximum from sample 1 can be attributed to differences in the chemical environment of the dye molecules in the two polymer matrices.

Figure 4 provides no immediately accessible information on the difference in physical structure between the two samples. However, close inspection of the spectra shows that the relative intensity of the two peaks in Figure 4a remains constant with increasing modulation frequency, whereas in Figure 4b the relative intensity of the feature centered at 626 nm increases with respect to the feature of 394 nm. These variations arise because of the different distributions of the chromophores within the sample. This is more clearly illustrated in Table I which lists the relative intensities of the absorption features over a wider range of modulation frequencies. The results are in good agreement with the Rosencwaig–Gersho theory special cases (*2*, *12*), which would suggest that the photoacoustic signal from the bulk dye should exhibit an $\omega^{-3/2}$ modulation frequency dependence whereas the surface film should exhibit a ω^{-1} dependence.

Figure 5 shows the impulse responses for the two samples recorded at the absorption maxima of the various spectral features. The absorption features assigned to the bulk dye in sample 1 both exhibit a broad impulse response reaching a maximum after approximately 6 ms and decaying fully after approximately 50 ms. The impulse response is of a form which has been observed to be typical of a sample containing an evenly distributed chromophore and with a relatively low optical density. In sample 2, the impulse response of the bulk dye absorption feature is of a similar form to that seen in sample 1. In contrast the impulse response of the feature

Table I. Variation of the Ratio of Photoacoustic Signal Amplitudes with Modulation Frequency for Samples 1 and 2

modulation freq Hz	sample 1[a]	sample 2[b]
15	1.28	1.96
25	1.28	2.14
35	1.28	2.24
45	1.23	2.28
55	1.23	2.37
65	1.23	2.47
75	1.21	2.48
85	1.23	2.50
95	1.19	2.44

[a] Ratio of the uncorrected PA signal amplitude at 560 and 412 nm. [b] Ratio of the uncorrected PA signal amplitude at 626 and 394 nm.

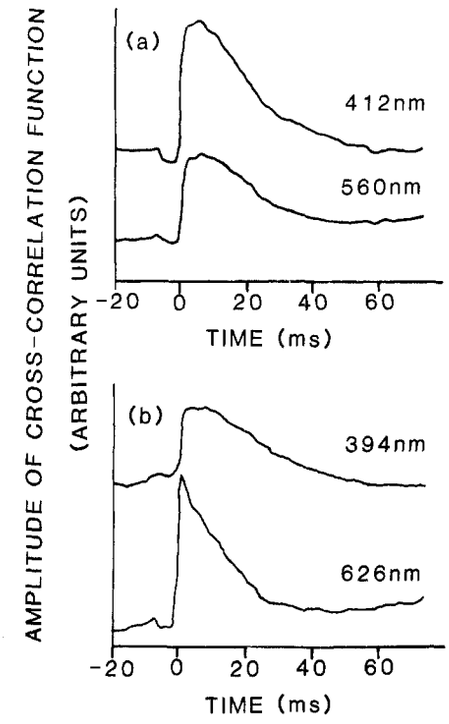

Figure 5. Comparison of impulse responses for dyed polymer films at different wavelengths: (a) bulk-dyed polymer film at 412 nm and 560 nm, (b) bulk-dyed polymer film with surface coating at 394 nm and 626 nm.

assigned to the surface coating is much sharper, peaking after 0.8 ms and decaying in approximately 25 ms. The results obtained can be understood intuitively. A thin absorbing layer at the surface of a sample will give rise to a highly localized source of heat when excited by a pulse of light; this will rapidly conduct into the bulk of the sample and across the sample boundary into the surrounding gas producing the photoacoustic signal. The signal would therefore be expected to peak rapidly and decay quickly. However, a chromophore distributed through the bulk of the sample will give rise to a widely distributed heat source and a correspondingly broader impulse response. The impulse response results provide a quick visual indication of the chromophore distribution and are therefore easier to interpret than the conventional PAS data.

A further example of the ability of the IMPAS technique to obtain depth related information is shown in Figure 6. This shows the impulse responses obtained from finely divided carbon black and erbium oxide at a wavelength of 522 nm. Both samples are very strongly absorbing at this wavelength; however, the impulse responses show that the photoacoustic

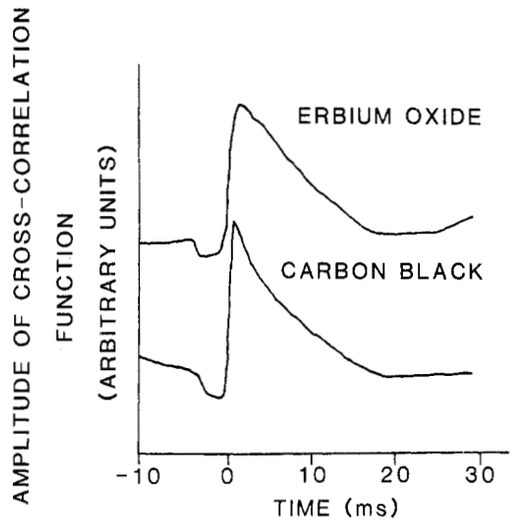

Figure 6. Comparison of the impulse responses obtained for carbon black and erbium oxide at 522 nm.

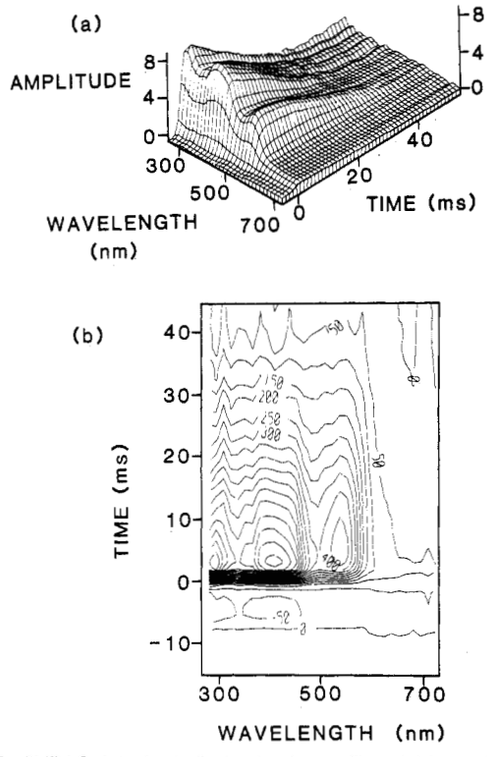

Figure 7. IMPAS data for bulk-dyed polymer film: (a) isometric projection, (b) contour map.

signal derives from a somewhat thicker layer in the erbium oxide than in the carbon black. This implies that the optical penetration depth is greater for the erbium oxide than for the carbon black. Thus, although both samples are "photoacoustically saturated", some information on relative absorption coefficients can be obtained.

The results given so far have shown only single impulse responses. Clearly, it is possible to obtain a whole series of impulse responses spread across a wavelength range, which could be displayed so as to represent depth and wavelength information simultaneously. The two simplest ways of presenting the data are as an isometric projection of a three-dimensional surface or as a contour map.

Figure 7a shows the three-dimensional surface derived from the IMPAS results obtained from sample 1 for 32 wavelengths in the range 265–730 nm at 15-nm intervals. The x axis shows wavelength, the y axis time, and the z axis the correlation

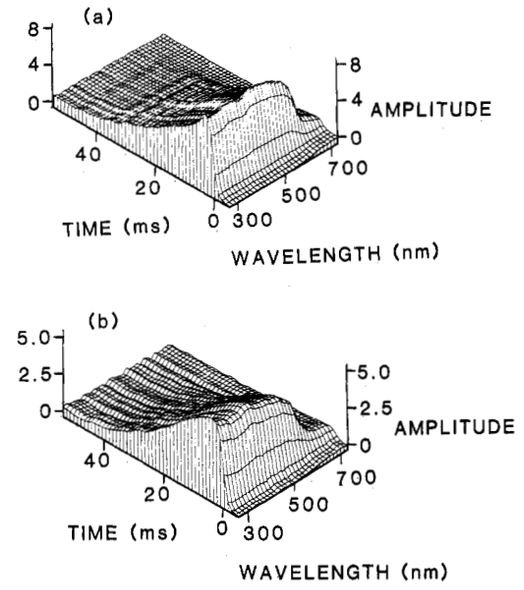

Figure 8. Isometric projection of the IMPAS data for an acetate film coated with a surface layer of red pigment: (a) original sample, (b) sample overcoated with a transparent polymer film.

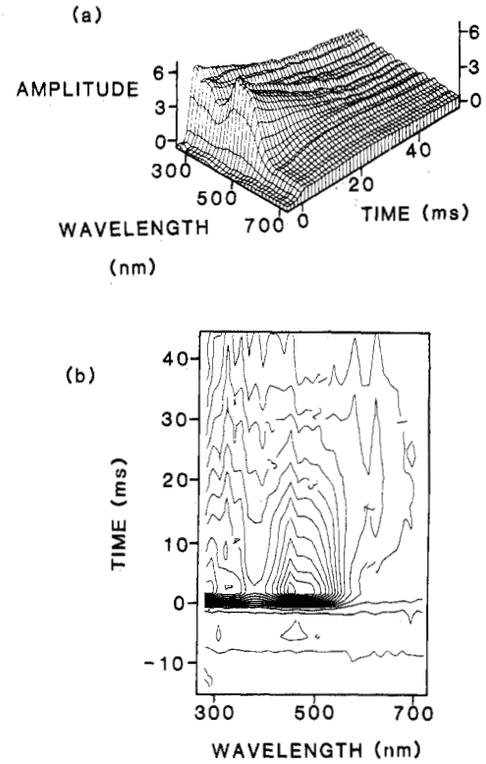

Figure 9. IMPAS data for a sample with two absorbing layers: (a) isometric projection, (b) contour map.

function (effectively signal intensity). The spectral structure is clearly seen and compares well with conventional PAS data shown in Figure 4a. However, the distortions of the isometric projection make quantitative measurements unreliable; small features can be concealed behind larger ones, and the determination of relative signal amplitudes is difficult. A more quantitative representation of the data can be obtained from a contour map of the data in which the contours pass through points of equal signal amplitude (Figure 7b). This representation does not convey the structure of the IMPAS data with the same immediacy as the isometric projection, but it does reveal features otherwise masked. Thus:

(1) The absorption feature centered at 280 nm is more intense than that of 412 nm.

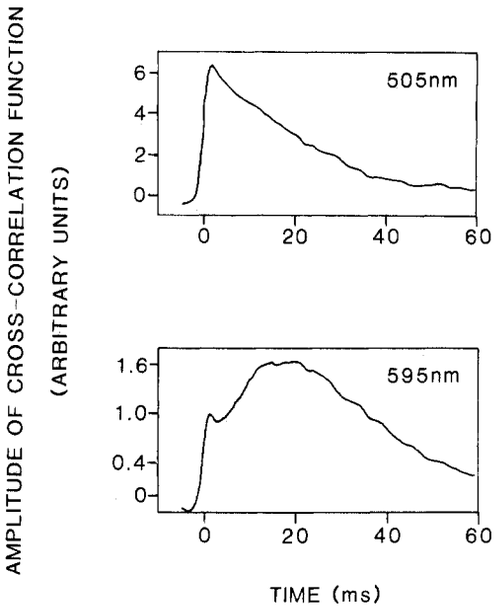

Figure 10. Comparison of the individual impulse responses for a two-layer sample at 505 nm and 595 nm.

(2) The distribution of absorption throughout the sample changes from band to band. It is clear from the contour map that for the absorption peak at 560 nm, light penetrates more deeply into the sample than at the other absorption peaks.

Figure 8 shows the isometric projections for a sample consisting of a transparent plastic film coated on one side with a thin layer of red pigment. Figure 8a shows the result obtained with the red layer uppermost in the cell. Figure 8b shows the result obtained with the surface covered by a layer of transparent self-sealing plastic film. It can be seen that the IMPAS results show no spectral differences between the two samples; however, the change in location of the chromophore can be detected in differences in the impulse responses. Figure 8b shows that for a sample with subsurface absorption, the amplitude of the response is reduced relative to the equivalent sample with surface absorption and the peak of the response is shifted to longer time delays. The reduction in amplitude arises from losses in the sample as the heat diffuses toward the surface and the shift in the response peak from the delay caused by the heat diffusing through the extra layer of plastic film. Thus, even though the optical density of the two samples was identical, it was possible to obtain information about the distribution of the chromophores.

This capability of IMPAS is extended to multilayer samples in Figure 9. The sample consisted of a black card substrate covered with a transparent acetate film 0.08 mm thick which was then coated with a thin layer of red pigment. Figure 9a shows the isometric projection of the data and Figure 9b the contour map. Figure 9a clearly shows the presence of the surface coating with an absorption spectrum tailing off at a wavelengths above 620 nm. In the region where the surface dye is not absorbing, it is possible to detect a slight bulge in the response surface at much longer time delays arising from light absorption at the film–substrate interface. The response is weak compared to the surface signal due to the relatively thick layer of acetate film and is masked by the larger features in this representation. The subsurface signal is much more clearly seen in the contour map, where a broad low peak can be detected at 625 nm. The presence of the subsurface feature is confirmed in Figure 10 which compares the single impulse responses obtained at 505 nm and 595 nm.

In several of the isometric projections of the IMPAS data, it is possible to observe ripples in the smooth decay of the impulse responses. These ripples are reproducible and occur at the same time delay across the full wavelength range used in the experiments. The ripples are attributed to defects in the PRBS modulator which produce cyclic errors in the pseudorandom sequence, leading to modulation of the light source with extra specific frequencies which are subsequently recovered by the correlation process.

CONCLUSIONS

IMPAS measurements greatly facilitate the study of samples with a depth variation in the distribution of chromophores. IMPAS provides information more quickly, and in more convenient form, than conventional PAS techniques using single frequency modulation. The technique shows considerable promise for the study of a wide variety of multilayer and thin film samples ranging from ceramic materials to polymers and biological systems.

ACKNOWLEDGMENT

The authors wish to acknowledge the assistance of I. P. Vickery and I. J. Flynn in the construction of the impulse response measurement system.

LITERATURE CITED

(1) Adams, M. J.; Beadle, B. C.; King, A. A.; Kirkbright, G. F. *Analyst (London)* **1976**, *101*, 553–561.
(2) Rosencwaig, A. "Photoacoustics and Photoacoustic Spectroscopy"; Wiley-Interscience: New York, 1980; pp 207–218.
(3) Buschmann, C.; Prehn, H. *Photobiochem. Photobiophys.* **1983**, *5*, 63–69.
(4) Mackenthun, M. L.; Tom, R. D.; Moore, T. A. *Nature (London)* **1979**, *279*, 265–266.
(5) Moore, T. A.; O'Hara, E. P.; Anjo, D. M.; Tom, R.; Benin, D. *J. Phys. (Orsay, Fr.)* **1983**, *44*, C6-339–345.
(6) Kirkbright, G. F.; Miller, R. M. *Anal. Chem.* **1983**, *55*, 502–506.
(7) Sugitani, Y. *Kagaku no Ryoiki* **1981**, *35*, 848–855.
(8) Sugitani, Y.; Uejimi, A.; Kato, K. *J. Photoacoust.* **1982**, *1*, 217–236.
(9) Davies, W. D. T. "System Identification for Self-Adaptive Control"; Wiley: London, 1970.
(10) Hieftje, G. M.; Haugon, G. R. *Anal. Chem.* **1981**, *53*, 755A–765A.
(11) Adams, M. J.; Beadle, B. C.; Kirkbright, G. F. *Analyst (London)* **1977**, *102*, 569–575.
(12) Rosencwaig, A.; Gersho, A. *J. Appl. Phys.* **1976**, *47*, 64–69.

RECEIVED for review February 27, 1984. Accepted May 21, 1984.